# Supporting Information

## Reinforcing Interfacial Molecular Dam through a Multifunctional Organic Electrolyte Additive for Stable Zn Anode

Zhenxin Lin, [a] Yufei Zhang, *[a, b] Xiaoting Lin, [a] Hanlin Ding, [a] Minghui Ye, [a, b] Zhipeng Wen, [a, b] Yongchao Tang, [a, b] Xiaoqing Liu [a, b] and Cheng Chao Li*[a, b]

[a] School of Chemical Engineering and Light Industry, Guangdong University of Technology, Guangzhou 510006, China.
[b] Guangdong Provincial Laboratory of Chemistry and Fine Chemical Engineering Jieyang Center, Jieyang 515200, China

Corresponding Authors at: School of Chemical Engineering and Light Industry, Guangdong University of Technology, Guangzhou 510006, China.
E-mail: yfzhang@gdut.edu.cn; licc@gdut.edu.cn

# Experimental Section

**Chemicals:**

$ZnSO_4 \cdot H_2O$ (AR) and $KMnO_4$(>99%) were purchased from Aladdin (Shanghai, China). 1,2,4-Triazole (>99%) was purchased from Macklin (Shanghai, China). Zn foil (99.95%) and Cu foil (99.95%) were purchased from Canrd Technology Co.

**Electrolyte preparation:**

The electrolytes were prepared by dissolving $ZnSO_4 \cdot 7H_2O$ and triazole (Ta) into deionized water (DI). Electrolyte with different Ta addition concentration were marked as 2 M $ZnSO_4$, 2 M $ZnSO_4$+0.05 M Ta, 2 M $ZnSO_4$+0.10 M Ta, 2 M $ZnSO_4$+0.20 M Ta, 2 M $ZnSO_4$+0.50 M Ta. The electrolyte with 2 M $ZnSO_4$+0.10 M Ta marked as Ta/$ZnSO_4$ for convenience.

**Synthesis of α-$MnO_2$:**

Firstly, $KMnO_4$ (0.329 g) was added to deionized (DI) water (38 mL) and stirred for 10 min. Then, HCl (1.4 mL) was continuously added in the above solution with stirring. The above mixture was transferred into the autoclave for hydrothermal treatment at 140 °C, 10 h. Finally, the products were collected and washed with DI water and alcohol several times, and vacuum dried at 60°C for 12 h.

**Materials characterization:**

The FT-IR spectra were obtained by an FT-IR spectrometer (Nicolet iS5, Thermo Scientific). The Raman spectra were collected by using the LabRAM HR Evolution Raman spectrometer. NMR spectra were provided with the NMR spectrometer (JNM-ECZ500R/S1, Japan). SEM images were carried out on the field-emission scanning electron microscope (Hitachi SU8220, Japan). XRD patterns were obtained with an X-ray diffractometer (D8 VENTURE, Bruker, Germany). XPS spectra were taken with the ESCALABMKLL X-ray photoelectron spectrometer (VG Instruments). The contact Angle measurement was performed on the OCA 100 (Data Physics) contact Angle meter. LCM images were taken with the Laser Scanning Confocal Microscopys (Olympus OLS4100). The Zeta values were measured by the Nano Particle Size and Zeta Potential Analyzer (Malvern Zetasizer Nano ZS).

**Electrochemical testing:**

Electrochemical performances of electrolytes were evaluated using CR2032 coin-type cells. The anode used a metal Zn foil with 100 μm thickness and the separator was Whatman GF/D glass microfibers paper. The electrochemical performance of the cell was measured using the Neware Electrochemical Test System (CT-4008-10V 50mA-164, Shenzhen, China). The cycling stability and Coulomb efficiency of Zn anodes in different electrolytes were evaluated by assembling Zn//Cu and Zn//Zn symmetric batteries with CR2032 coin-type batteries. For cathode preparation of the Zn//$MnO_2$ full cell, a slurry of $MnO_2$, black carbon and PVDF with the ratio of 7:2:1 were coated on stencil and the $MnO_2$ loading mass of the electrodes was about 1.2 mg $cm^{-2}$.

The cyclic voltammetry curves, corrosion curves and linear sweep voltammetry curves were obtained on a Gamry electrochemical bench with a three-electrode system (Zn foil as the working electrode, Pt as the counter electrode, and Ag/AgCl as the reference electrode). However, the electrochemical window was obtained by changing the working electrode, changing the Zn foil to Ti foil. The frequency range of electrochemical impedance spectroscopy (EIS) analysis was 0.01 ~ $10^6$ Hz, and the applied amplitude was 10 mV. All tests were conducted at room temperature.

**DFT calculation:**

We used the DFT as implemented in the Vienna Ab initio simulation package (VASP) in all calculations. The exchange-correlation potential is described by using the generalized gradient approximation of Perdew-Burke-Ernzerhof (GGA-PBE). The projector augmented-wave (PAW) method is employed to treat interactions between ion cores and valence electrons. The plane-wave cutoff energy was fixed to 450 eV. Given structural models were relaxed until the Hellmann–Feynman forces smaller than -0.02 eV/Å and the change in energy smaller than $10^{-5}$ eV was attained. Grimme's DFT-D3 methodology was used to describe the dispersion interactions among all the atoms in adsorption models.

The adsorption energy is defined as:

$$Eads = E(system)-E(catalyst) -E(species)$$

where E(system), E(catalyst), and E(species) are the total energy of the optimized system with adsorbed species, the isolated catalyst, and species, respectively.

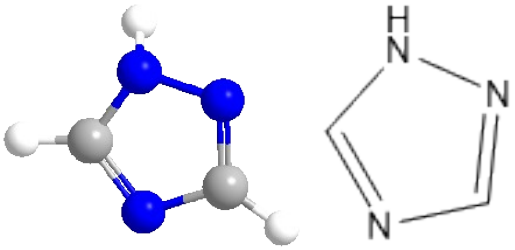


**Fig S1.** Structural formula of triazole.

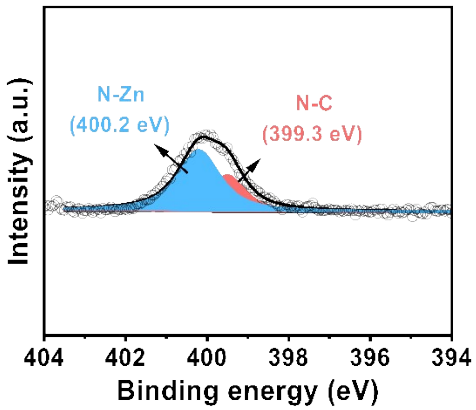


**Fig S2.** The high-resolution spectra of N 1s XPS spectra.

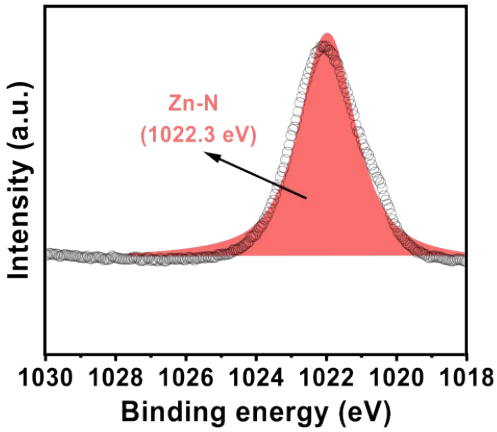


**Fig S3.** The high-resolution spectra of Zn 2p XPS spectra.

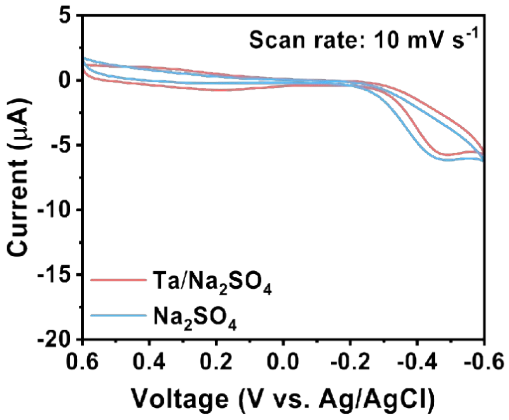


**Fig S4.** CV of 0.2 M $Na_2SO_4$ and 0.2 M $Na_2SO_4$ with 0.1 M Ta.

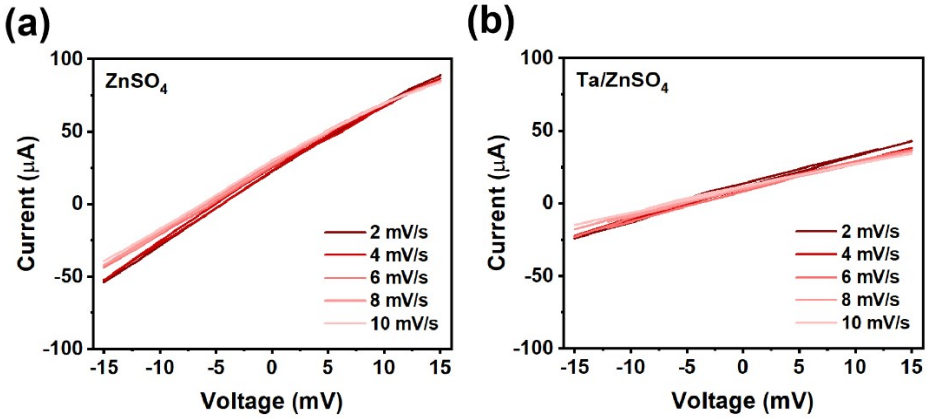


**Fig S5.** Evaluation on differential capacitances and CV of Zn anode in (a) $ZnSO_4$ and (b) Ta/$ZnSO_4$ electrolytes.

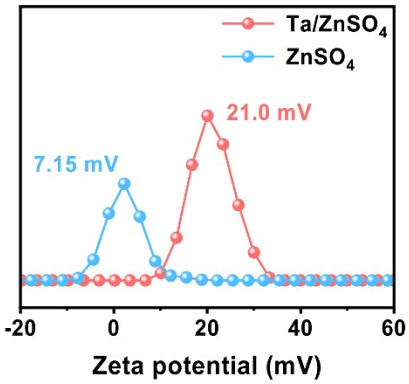


**Fig S6.** Zeta potential of zinc powder with and without Ta additive.

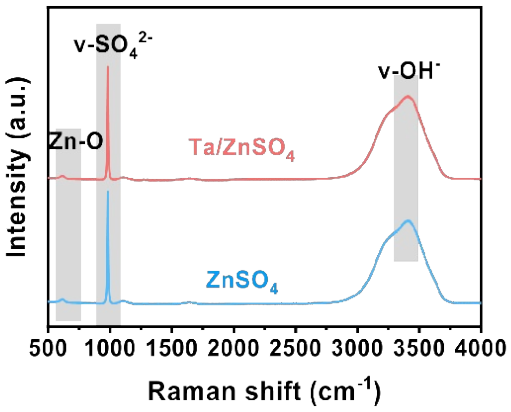


**Fig S7.** Raman of $ZnSO_4$ and Ta/$ZnSO_4$ electrolytes.

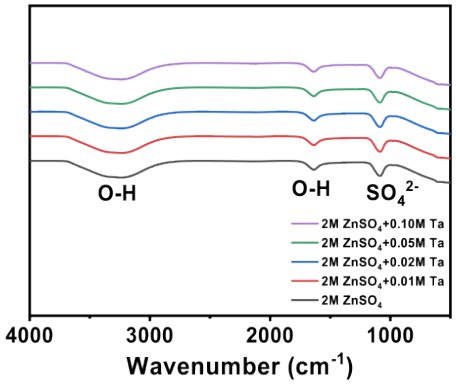


**Fig S8.** FTIR with different additive concentrations.

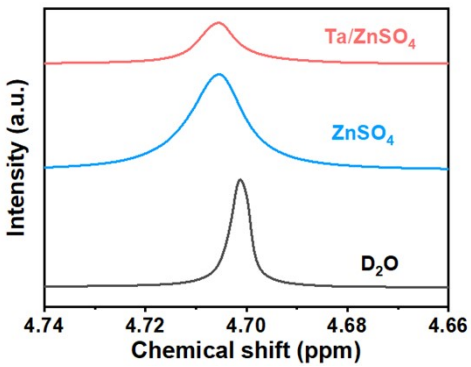


**Fig S9.** NMR of $ZnSO_4$ and Ta/$ZnSO_4$ electrolytes.

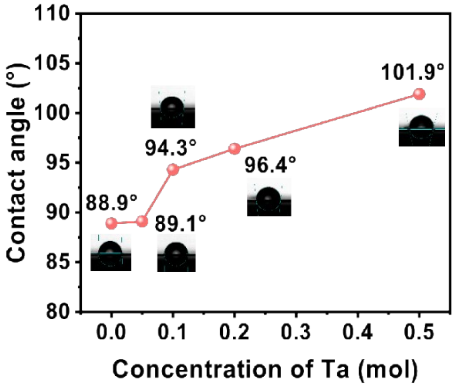


**Fig S10.** The effect of adding different amounts of Ta on the contact angle.

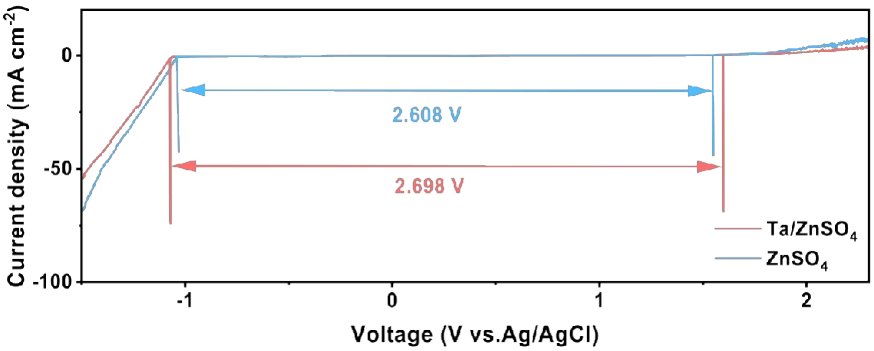


**Fig S11** Electrochemical windows of $ZnSO_4$ and $Ta/ZnSO_4$ electrolyte.

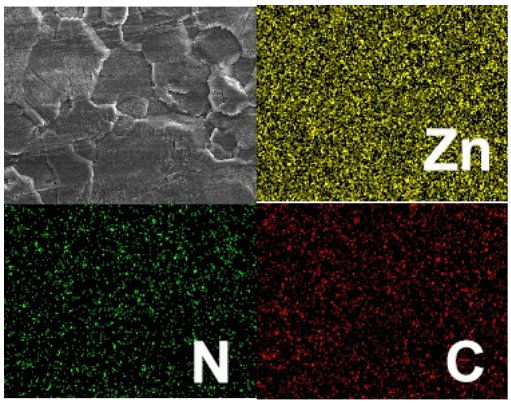


**Fig S12.** The EDS images of different elements on Zn foils after soaked in $Ta/ZnSO_4$ electrolyte for 7 days.

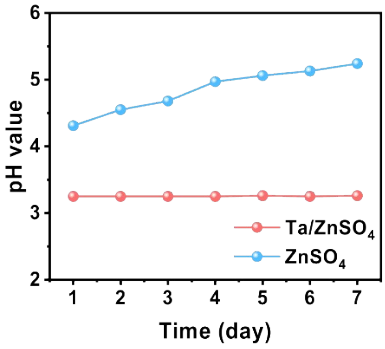


**Fig S13.** pH changes as function of immersion time with Zn electrode.

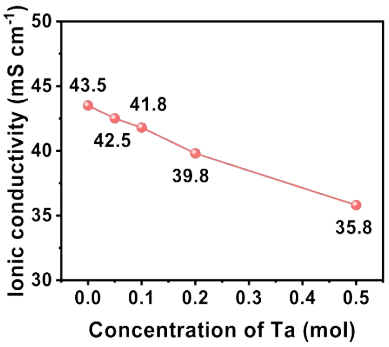


**Fig S14.** Changes in ionic conductivity with different amounts of Ta addition.

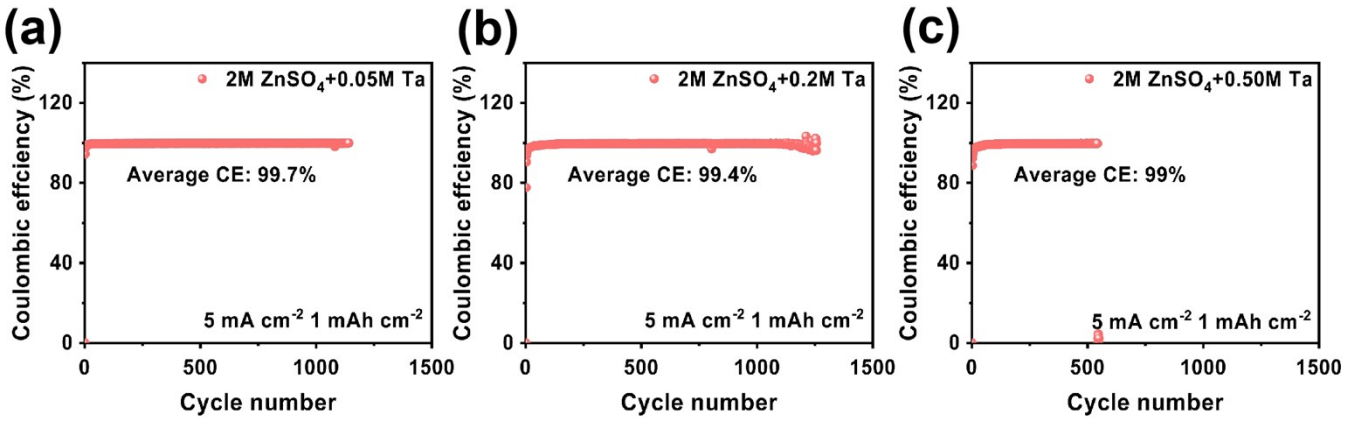


**Fig S15.** CE tests of Zn//Cu asymmetrical cells at 5 mA $cm^{-2}$ and 1 mAh $cm^{-2}$ in different additive concentration.

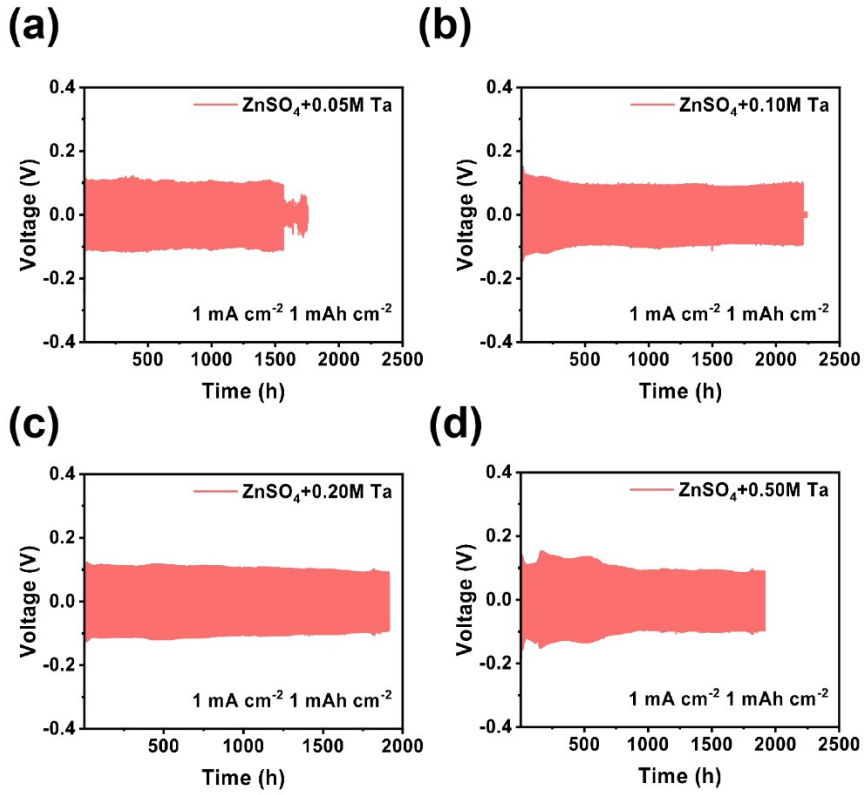


**Fig S16.** Symmetrical cells with different additive solubility.

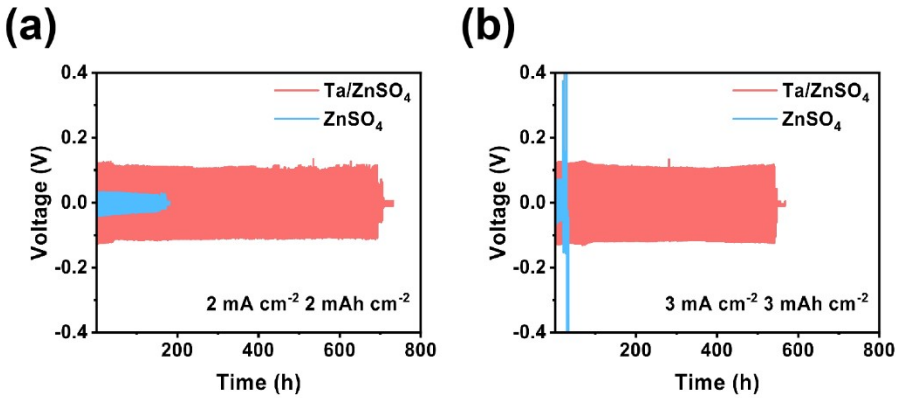


**Fig S17.** Symmetric cells of $Ta/ZnSO_4$ and $ZnSO_4$ at (a) 2 mA $cm^{-2}$, 2 mAh $cm^{-2}$ and (b) 3 mA $cm^{-2}$, 3 mAh $cm^{-2}$.

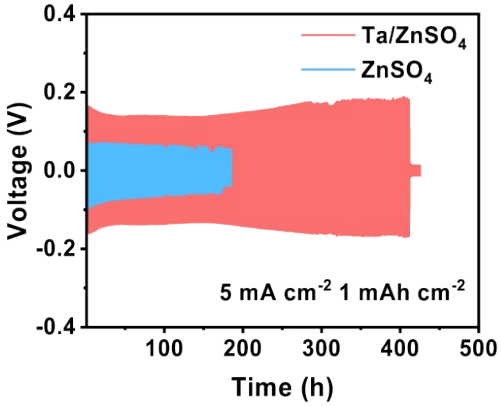


**Fig S18.** Symmetric cells of $Ta/ZnSO_4$ and $ZnSO_4$ at 5 mA $cm^{-2}$,1 mAh $cm^{-2}$.

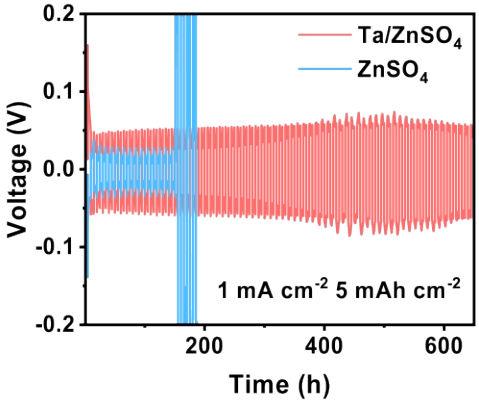


**Fig S19.** Symmetric cells of $Ta/ZnSO_4$ and $ZnSO_4$ at 1 mA $cm^{-2}$,5 mAh $cm^{-2}$.

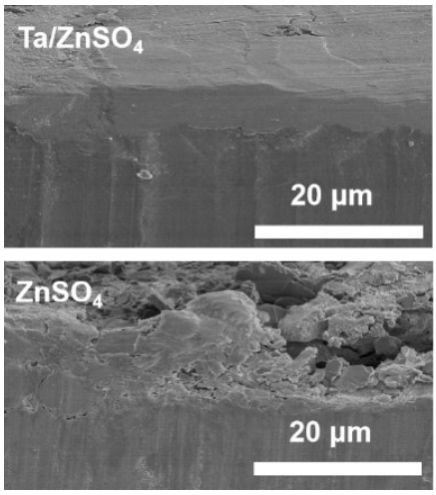


**Fig S20.** Cross sections of $Ta/ZnSO_4$ and $ZnSO_4$ electrolytes after 100 cycles.

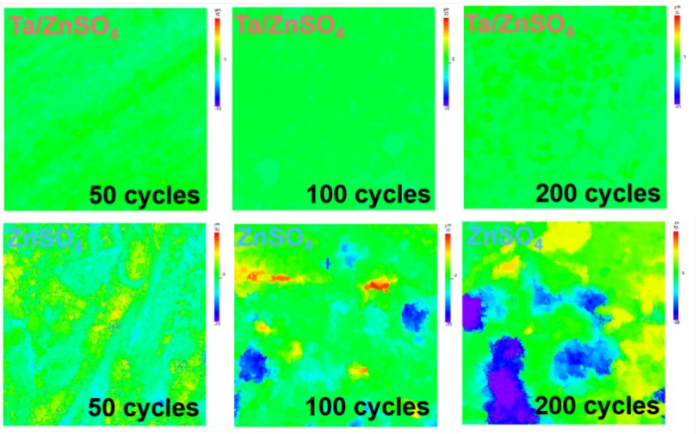


**Fig S21.** LCM-2D images of Zn deposited in different cycles of $ZnSO_4$ and $Ta/ZnSO_4$ electrolytes.

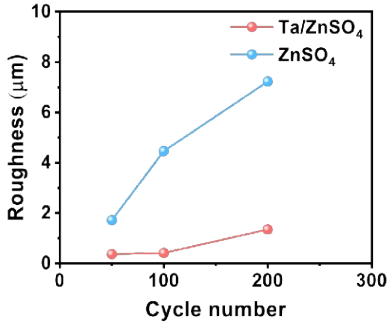


**Fig S22.** Roughness of Zn deposited in $ZnSO_4$ and $Ta/ZnSO_4$ electrolytes of different cycles.

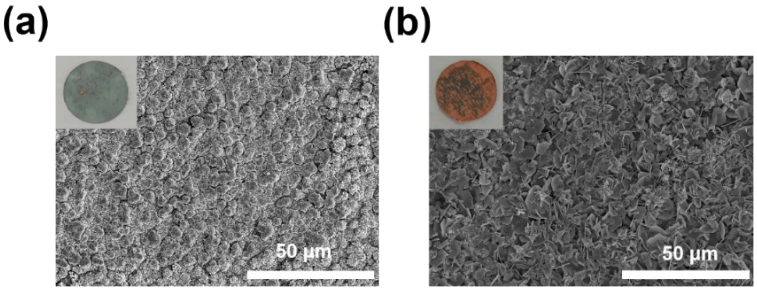


**Fig S23.** SEM images of Zn deposition on Cu foil in different electrolytes.

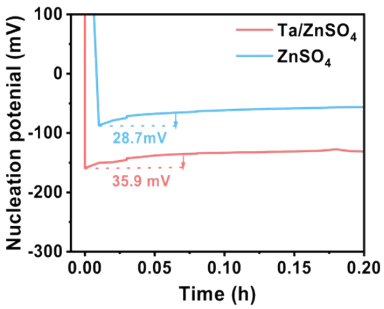


**Fig S24.** Nucleation overpotential of Zn deposition on Cu foil in $Ta/ZnSO_4$ and $ZnSO_4$ electrolytes.

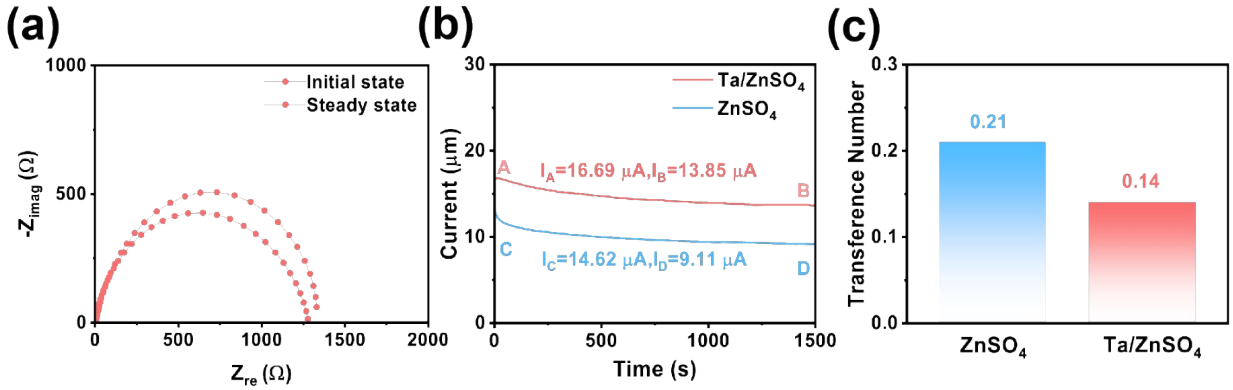


**Fig S25.** Ion migration numbers in Ta/$ZnSO_4$ and $ZnSO_4$ electrolytes.

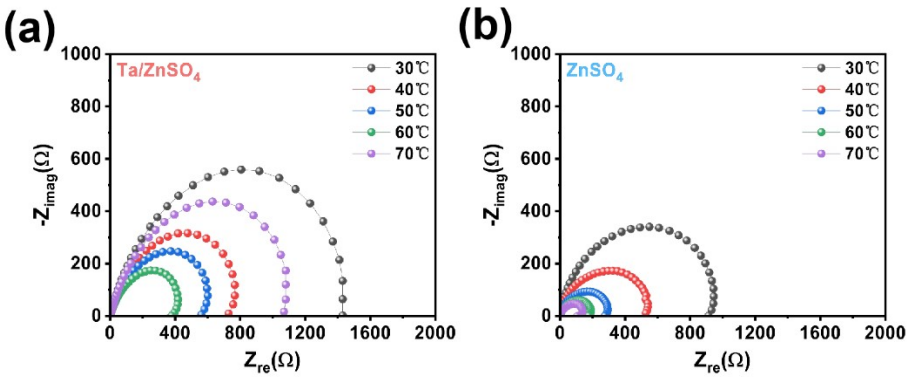


**Fig S26.** Nyquist plots of Ta/$ZnSO_4$ and $ZnSO_4$ electrolytes at different temperatures.

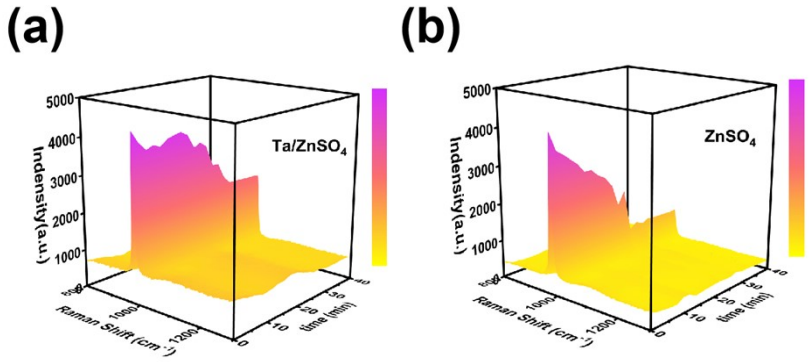


**Fig S27.** 3D plot of Raman intensity variation during Zn deposition.

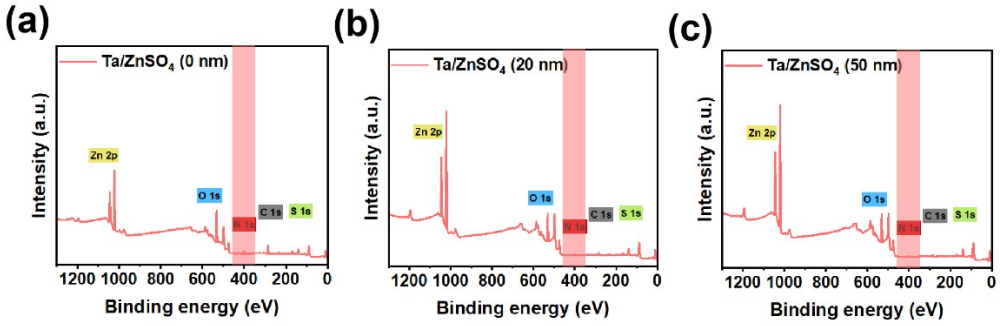


**Fig S28.** XPS depth profile of Zn anode after 200 h.

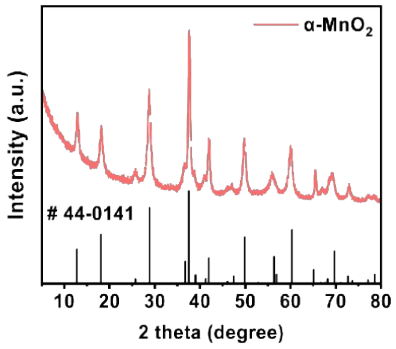


**Fig S29.** XRD pattern of the as-prepared α-$MnO_2$ nanobelts.

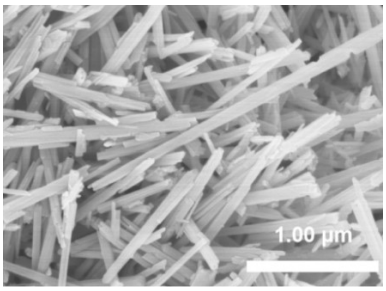


**Fig S30.** SEM image of the as-prepared α-$MnO_2$ nanobelts.

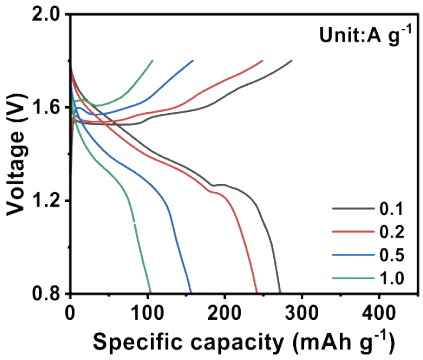


**Fig S31.** Capacity-voltage profiles of Zn//α-$MnO_2$($ZnSO_4$) at different current densities.

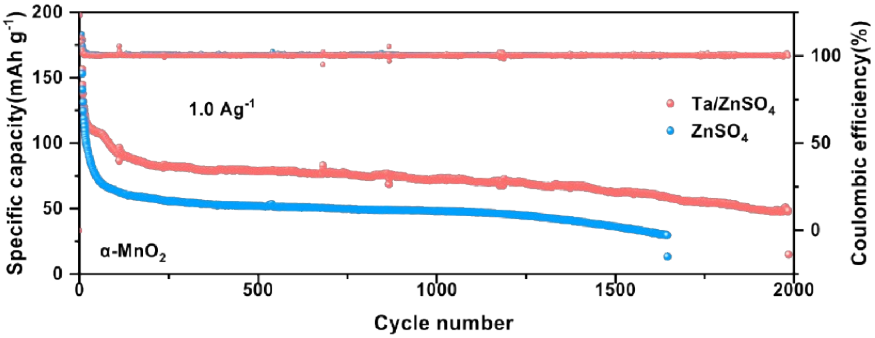


**Fig S32.** Cycling stability of Zn//α-$MnO_2$ ($ZnSO_4$) and Zn//α-$MnO_2$ (Ta/$ZnSO_4$) at 1.0 A $g^{-1}$.

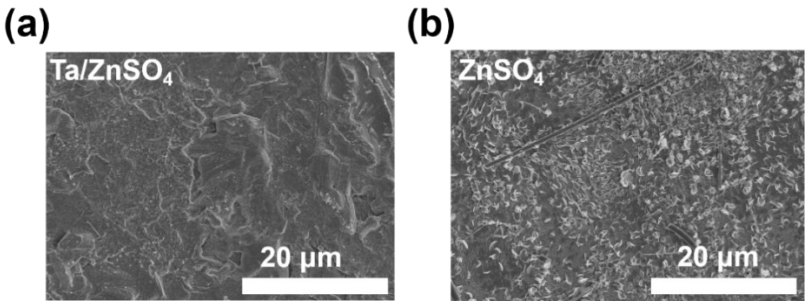


**Fig S33.** The SEM images of Zn anode in Zn//α-$MnO_2$ ($ZnSO_4$) and Zn//α-$MnO_2$ (Ta/$ZnSO_4$) full cells after 100 cycles of cycling.

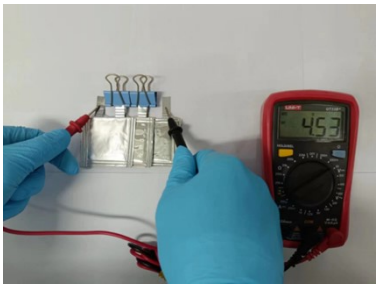


**Fig S34.** The voltage of flexible quasi-solid-state Zn//α-$MnO_2$(Ta/$ZnSO_4$) cells.

## Captions for Supporting Videos

**Video S1.** In situ optical video of the electroplating behavior of $Zn^{2+}$ on the Zn cathode of a symmetric Zn//Zn cell with $ZnSO_4$ electrolyte under discharge conditions at a current density of 1 mA $cm^{-2}$ for 40 min.

**Video S2.** In situ optical video of the electroplating behavior of $Zn^{2+}$ on the Zn cathode of a symmetric Zn//Zn cell with Ta/$ZnSO_4$ electrolyte under discharge conditions at a current density of 1 mA $cm^{-2}$ for 40 min.